



U.S. DEPARTMENT OF  
**ENERGY**

PNNL-17514

Prepared for the U.S. Department of Energy  
under Contract DE-AC05-76RL01830

# **FY07 Annual Report: Amorphous Semiconductors for Gamma Radiation Detection (ASGRAD)**

BR Johnson  
BJ Riley  
JV Crum  
SK Sundaram  
C Henager

C Seifert  
R Van Ginhoven  
A Rockett, UIUC

January 2008



**Pacific Northwest**  
NATIONAL LABORATORY

*Proudly Operated by **Battelle** Since 1965*

## DISCLAIMER

This report was prepared as an account of work sponsored by an agency of the United States Government. Neither the United States Government nor any agency thereof, nor Battelle Memorial Institute, nor any of their employees, makes **any warranty, express or implied, or assumes any legal liability or responsibility for the accuracy, completeness, or usefulness of any information, apparatus, product, or process disclosed, or represents that its use would not infringe privately owned rights.** Reference herein to any specific commercial product, process, or service by trade name, trademark, manufacturer, or otherwise does not necessarily constitute or imply its endorsement, recommendation, or favoring by the United States Government or any agency thereof, or Battelle Memorial Institute. The views and opinions of authors expressed herein do not necessarily state or reflect those of the United States Government or any agency thereof.

PACIFIC NORTHWEST NATIONAL LABORATORY

*operated by*

BATTELLE

*for the*

UNITED STATES DEPARTMENT OF ENERGY

*under Contract DE-ACO5-76RL01830*

This work was conducted in part at the Environmental Molecular Sciences Laboratory (EMSL), which is operated by the Office of Biological and Environmental Research of the U.S. Department of Energy (DOE) at Pacific Northwest National Laboratory (PNNL).

Printed in the United States of America

Available to DOE and DOE contractors from the  
Office of Scientific and Technical Information,  
P.O. Box 62, Oak Ridge, TN 37831-0062;

ph: (865) 576-8401

fax: (865) 576 5728

email: [reports@adonis.osti.gov](mailto:reports@adonis.osti.gov)

Available to the public from the National Technical Information Service,  
U.S. Department of Commerce, 5285 Port Royal Rd., Springfield, VA 22161

ph: (800) 553-6847

fax: (703) 605-6900

email: [orders@nits.fedworld.gov](mailto:orders@nits.fedworld.gov)

online ordering: <http://www.ntis.gov/ordering.htm>

## **FY07 Annual Report: Amorphous Semiconductors for Gamma Radiation Detection (ASGRAD)**

B. R. Johnson  
B. J. Riley  
J. V. Crum  
S. K. Sundaram  
C. Henager  
C. Seifert  
R. Van Ginhoven  
A. Rockett, UIUC

January 2008

Work performed for the Office of Defense Nuclear Nonproliferation (NA-20)  
Office of Nonproliferation Research and Development (NA-22) under  
Project Number PL06-136-PD05

Prepared for the U.S. Department of Energy  
under Contract DE-AC05-76RL01830

Pacific Northwest National Laboratory  
Richland, Washington 99354

# Summary

We describe progress in the development of new materials for portable, room temperature, gamma-radiation detection at Pacific Northwest National Laboratory. High Z, high resistivity, amorphous semiconductors are being designed for use as solid-state detectors at near ambient temperatures; their principles of operation are analogous to single-crystal semiconducting detectors. Compared to single crystals, amorphous semiconductors have the advantages of rapid, cost-effective, bulk-fabrication; near-net-shape fabrication of complicated geometries; compositional flexibility; and greater electronic property control. The main disadvantage is reduced-charge carrier mobility. The focus of this project is to develop optimized amorphous semiconductor materials for gamma detection applications that leverage their material advantages while mitigating their limitations.

During the second year of this project, several important milestones were accomplished. Major accomplishments were:

- 1) Significant processing – property and composition – property correlations were determined for Cd-Ge-As glasses.
- 2) Radiation response testing was successfully demonstrated on three different amorphous semiconductor materials (Cd-Ge-As, As-Se, and As-Se-Te systems) at ambient and near ambient temperatures.
- 3) Advanced, enabling Schottky contacts were developed for Cd-Ge-As compounds. This will allow these materials to perform at ambient temperatures.
- 4) The collaborative working relationship developed with Prof. Angus Rockett at the University of Illinois at Urbana-Champaign (UIUC) has continued to grow, and they are credited with several of the materials characterization and contact development successes achieved this year.

The development of Schottky barrier contacts in amorphous semiconductors by simply using different types of metal contacts is very significant. This is because these structures allow us to fabricate functional diodes using the Schottky barrier as the “blocking” contact, similar to the familiar silicon surface barrier detector. In device terms, lower resistivity materials with better charge carrier mobility properties can be used and operated under reverse bias to create a low-noise, high-resistivity condition that can be switched to a low-resistivity, high conductivity condition under exposure to radiation events, and then off again. In the future, lithographic techniques could be used to create an array of FET's, and thereby build pixilated detectors that would have 2D position-sensitive radiation detection capability.

Thus, the third year of the project will be dedicated to building diode-based devices from these amorphous semiconductors. The major challenges to date with the Schottky contacts have been a large variation in device behavior from contact to contact, and the relative fragility of the contacts. We are developing strategies to solve these issues. Additionally, particular emphasis will be directed towards characterizing device performance in response to ionizing radiation, which is key to demonstrating the viability of amorphous semiconductor-based detectors.



## Abbreviations and Acronyms

BSE	Back-scattered electron
CVD	Chemical vapor deposition
DSC	Differential scanning calorimeter
DTA	Differential thermal analysis
EDS	Energy dispersive spectroscopy
EMSL	Environmental Molecular Sciences Laboratory
FET	Field effect transistor
FTIR	Fourier transform infrared
IBA	Ion beam analysis
IR	Infrared
IV	Current - voltage
NIST	National Institute for Standards and Technology
NOMSL	Non-oxide Materials Synthesis Laboratory
PIXE	Particle-induced X-ray emission
PNNL	Pacific Northwest National Laboratory
RBS	Rutherford backscattering
SEM	Scanning electron microscopy
SOW	Statement of work
STA	Simultaneous thermal analysis
TGA	Thermogravimetric analysis
UHV	Ultra-high vacuum
UIUC	University of Illinois at Urbana-Champaign
UV-VIS-NIR	Ultraviolet visible near infrared
XRD	X-ray diffraction
Z	Atomic number



# Contents

1.0	Introduction.....	1.1
2.0	Thermal Processing Advancements .....	2.1
2.1	Water quenched double-containment ampoules.....	2.1
2.2	Liquid gallium quenched single-walled ampoules .....	2.2
2.3	New Chemistries.....	2.3
2.4	Processing Summary.....	2.4
3.0	Discovery of New Metastable Phase.....	3.1
4.0	Radiation Response Testing: Sealed Alpha Sources .....	4.2
4.1	Current-voltage curves.....	4.2
4.2	DC ionization experiments.....	4.3
4.3	Summary.....	4.5
5.0	Collaboration With the University of Illinois at Urbana-Champaign (UIUC).....	5.1
5.1	Samples analyzed.....	5.1
5.2	Electrical measurements.....	5.1
5.3	Optical measurements.....	5.3
5.4	X-ray diffraction .....	5.4
5.5	Microchemistry.....	5.5
5.6	Conclusions of the materials characterization at UIUC.....	5.7
5.7	Schottky contacts .....	5.8
6.0	Strategy and Future Direction .....	6.1
6.1	Strategy.....	6.1
6.2	Future Direction.....	6.1
7.0	References.....	7.1

## Figures

Figure 1. Top: double containment schematic; Bottom: double containment ampoule with copper.....	2.1
Figure 2. Thermal conductivity of different metals (Lide 2007). .....	2.2
Figure 3. Liquid gallium in an alumina crucible at ~150°C. ....	2.3
Figure 4. Plot of density and conductivity as a function of Te concentration for $As_{40}Se_{(60-x)}Te_x$ [7,8]....	2.3
Figure 5. Optical absorption coefficient plots as a function of photon energy for $CdGe_xAs_2$ glass. (A) double-containment (DC) quench method; (B) liquid Ga quench method; (C) DC vs. liquid Ga quench method; (D) effect of $H_2$ doping for samples made via liquid Ga quench process. ....	2.4
Figure 6. Microscopic analysis of metastable phases formed in Cd-Ge-As during quenching. Polarized reflected light microscopy (A) revealed two distinct crystal morphologies (polycrystals and needles) in an amorphous matrix. Examination by XRD detected $CdGeAs_2$ and a new, unidentified phase(s). Electron backscattered diffraction (B) determined the polycrystals (colored) were $CdGeAs_2$ , and confirmed the matrix was amorphous, but diffraction patterns from needles were unidentifiable. Compositional differences ( $Z_{ave}$ contrast) were accentuated using SEM BSE (C), and stoichiometry was determined by quantitative EDS mapping (D, polycrystals = $CdGeAs_2$ , needles = $Cd_3Ge_2As_4$ ). Lattice parameters, space group, and structure factor calculations for the new phase are in progress.	3.1
Figure 7. Current-voltage curve for $CdGe_{0.85}As_2$ from 0-100 V at $-40^\circ C$ .....	4.2
Figure 8. Current vs. time for $As_{40}Se_{48}Te_{12}$ as a function of exposure to a sealed source at room temperature and a bias of 500V.....	4.3
Figure 9. Variation in DC ionization current as a function of applied field.....	4.4
Figure 10. Detector gain as a function of applied field for amorphous $As_2S_3$ for exposure to a sealed alpha source. ....	4.5
Figure 11. (A) Current-voltage measurements contact to contact across two samples, polycrystalline ASGRAD 5 and amorphous ASGRAD 23. (B) The resistances calculated as a function of voltage from the data in (A).....	5.2
Figure 12. Typical optical transmission/ reflection data results for sample ASGRAD 23.....	5.3
Figure 13. Typical ellipsometry data for several samples. The values to the left of the ASGRAD number in the legend is the Ge fraction, x, in the $CdGe_xAs_2$ .....	5.4
Figure 14. X-ray diffraction data for four samples including one polycrystalline sample (light blue), one partially crystalline (yellow), and two amorphous (ASGRAD 23 and ASGRAD 31c). Each data set was fit with a series of Gaussian curves (black). The fit example was for the ASGRAD 31c. Spectrum for the glass specimen holder is included as evidence that the instrument did not contribute to the data.....	5.5
Figure 15. (Left) The valence band of ASGRAD 30 measured with HeI and HeII photons. The valence states likely responsible for the major transitions are labeled. (Right) Same HeI valence band spectrum as on Left, but plotted on a logarithmic scale showing the states near the Fermi energy .	5.6
Figure 16. A test pattern and contact arrays of Mg metal deposited on Sample ASGRAD 41c. Current - voltage measurements were made from Mg contact to Mg contact, from Mg contact to an ohmic	

contact (used for Hall effect) on the back side of the wafer, and from Mg contact to a probe placed directly on an exposed area of the CGA..... 5.8

Figure 17. Left, a linear scale plot and right a logarithmic plot of the current/voltage curves for sample 41c measured between two sets of Mg contacts in the light and in the dark. A large difference in conductivity is observed..... 5.9

## Tables

Table 2.1. Summary of ampoules produced in FY07 ..... 2.5

Table 5.1 Samples analyzed at UIUC and analysis results summary. .... 5.1

# 1.0 Introduction

The guiding motivation of this project is to develop new, innovative materials to enable detection of gamma radiation. The two principal techniques used to detect and obtain energy resolution information from gamma radiation are based on either scintillators or semiconductors. This project chose to focus on the second – the direct conversion of gamma photons into an electrical signal using semiconductors. Traditional semiconductor-based detectors rely on single crystals as the active detecting medium because they have a well-ordered electronic structure that facilitates rapid charge carrier transport. However, there are significant processing problems associated with the growth of large ( $\sim 1\text{cm}^3$ ), defect-free, single crystals from multi-component materials (e.g., Cd-Zn-Te (CZT) crystals). These challenges limit the size and availability of the crystals for applications. A significant amount of research and development is still required to improve the performance and production yield of single crystal CZT.

In light of this need, we have proposed the development of amorphous semiconductors as a potential alternative or interim solution for room-temperature gamma radiation detection. Compared to single crystals, amorphous semiconductors have the potential advantages of rapid, cost-effective, bulk-fabrication; near-net-shape fabrication of complicated geometries; compositional flexibility, and greater compositional and electronic property control. The main disadvantage of an amorphous semiconductor is reduced-charge carrier mobility due to the disordered structure. In this project, we are focusing our efforts to mitigate the technical problems with amorphous semiconductors to develop an optimized material for radiation detection. We will address the limited mobility issue in three ways:

- First, we will use processing and compositional modifications to minimize the population density of defect states near the band edges and in the mobility gap to maximize mobility.
- Second, we will design devices with high bias voltage fields ( $\geq 10^4$  V/cm) to take advantage of tunneling and avalanche gain effects to compensate for lost charge carriers.
- And, third, we will use photolithographic patterning and Schottky barrier contacts to create pixilated FET structures with reduced transit distances to minimize charge collection times. We have already made significant progress on the first two issues. We will continue to tackle these and the third issue in to the future.

The materials selected for this study were based on the following criteria: semiconducting, moderate-to-high atomic number, moderate band-gap, high-resistivity, and glass forming. This lead us to two families of amorphous semiconductors – the chalcogenides (compounds based on S, Se, or Te) and the chalcopyrites (a class name given to a family of component compounds that have a tetragonal unit cell) Within the chalcopyrite family of semiconductors, CdGeAs<sub>2</sub> is the best-known glass-former. Single crystal CdGeAs<sub>2</sub> has very excellent charge carrier mobility ( $\sim 10^4\text{cm}^2/(\text{Vs})$  at room temperature) [1,2], and has one of the highest reported non-linear optical coefficients. It is also iso-structural with another multi-component single crystal chalcopyrite semiconductor, AgGaSe<sub>2</sub>, which has demonstrated radiation detection capability [3]. In the amorphous form, CdGeAs<sub>2</sub> has a large reported compositional range (Ge = 0.2 - 1.3) and also has reported substitutional ability (e.g. replace Ge with other elements such as Si or Sb) [4-6]. These properties make it a very good candidate for investigating the potential application of amorphous semiconductors for radiation detection applications. Unfortunately, its band gap ( $\sim 0.9 - 1.0$  eV) and its resistivity ( $10^7 - 10^9$  Ohm-cm) are somewhat lower than optimal. However, because it is a known multi-component, glass-forming semiconductor, it lies within the targeted region of the periodic table, and it has very large compositional flexibility, it is a good material to demonstrate compositional control of gamma radiation detection properties. Additionally, the fact that it is iso-structural with other

higher Z chalcopyrites such as AgGaSe<sub>2</sub> (that has been reported to respond in crystal form to gamma radiation) may allow us to blend these compounds together in an amorphous state to create an ideal amorphous gamma radiation detection material.

The chalcogenide family of amorphous semiconductors from the As-Se-Te system was chosen not only because of their electrical properties, but because they are excellent glass formers, they are exceptionally resistive ( $\geq 10^{12}$  ohm•cm), and they are sensitive to optical photons (photo-induced property changes). It was suspected that their photosensitivity might be an indication of being sensitive to ionizing radiation as well (gamma photons).

The major successes in FY06 were processing based: we developed the ability to synthesize crack-free, amorphous ingots of Cd-Ge-As glass with very high purity and homogeneity. Two different process methods were developed, and various physical, chemical, and electrical analyses were completed to establish the homogeneity and chemical purity of the material. Initial testing and evaluation these material established they had suitable properties for radiation detection applications.

In FY07, we were able to move beyond transforming raw elements to new materials, into actually making and testing devices made from these new materials. The major successes in FY07 are as follows:

- We demonstrated the ability to measure a DC ionization response to alpha radiation in three different amorphous semiconductors: CdGe<sub>0.85</sub>As<sub>2</sub>, As<sub>40</sub>Se<sub>60</sub>, and As<sub>40</sub>Se<sub>48</sub>Te<sub>12</sub>.
- We demonstrated the ability to control and reduce the density of defect states in the band gap of Cd-Ge-As glasses by controlling composition as well as processing conditions.
- We demonstrated the ability to reduce the density of defect states by doping the material with hydrogen, a commonly used approach when working with amorphous silicon.
- We were able to build Schottky barrier contacts on Cd-Ge-As glass and demonstrated diode performance and enhanced photosensitivity. The barrier contacts reduced the leakage currents by approximately 5 orders of magnitude. This enabled the ability to measure a photoconductive response in the material: the illuminated conductivity was about 2 orders of magnitude greater than in the dark.

For FY08, our intent is to build upon the past successes and demonstrate the radiation response of these materials to discrete pulse signals from alpha and gamma sources. Our strategy to accomplish this is as follows:

- We will acquire higher precision electrical testing equipment. The high resistivities and small signals ( $\leq 10$  nA) necessitate the use of sophisticated electrometers, source meters, pre-amps, and signal processing units to make accurate measurements.
- Design and build more sophisticated devices to include such features as guard rings and pixilated contacts for enhanced radiation detector performance. We will perform basic electrical characterization of these devices to determine their performance parameters (bias voltage, time constant, etc.) for radiation testing, and then perform radiation tests on them.
- We will work to develop Schottky barrier contacts on Cd-Ge-As glass to build bulk devices that can be operated at high biases with low leakage current noise. Initial electrical testing results are promising as well as their high degree of photosensitivity.

The data obtained during FY08 should provide a reasonable understanding of the performance envelope of these materials. This information will allow one to design suitable devices and identify suitable applications for using amorphous semiconductor-based radiation detectors.

## 2.0 Thermal Processing Advancements

One of the key milestones of success in the project was the ability to form bulk, crack-free ingots of Cd-Ge-As glass. We were able to develop two different methods to accomplish this.

### 2.1 Water quenched double-containment ampoules

One approach to fabricating amorphous, crack-free ampoules was to use a double-containment system. Two concentric, evacuated ampoules are used; the inner is filled with the elements of choice, and the gap between the inner and outer is filled with a high thermal conductivity material (e.g. Cu). The approach has several advantages. The increased thermal mass of the system reduces the heat loss during transfer of the ampoule from the furnace to the quench bath. It is possible for the onset of nucleation to occur quite rapidly, so it is important to make the temperature change from furnace to quench bath as steep as possible. For the quench process, the Cu filler provides high thermal conductivity and rapid, uniform cooling throughout the ingot. Additionally, the Cu powder sinters during thermal processing, and provides an additional constraint on the ingot that inhibits volumetric expansion upon crystallization (the amorphous phase is more dense than the crystalline). A cartoon of the design is shown in Figure 1. A plot of thermal conductivity as a function of temperature for various materials is shown in Figure 2.

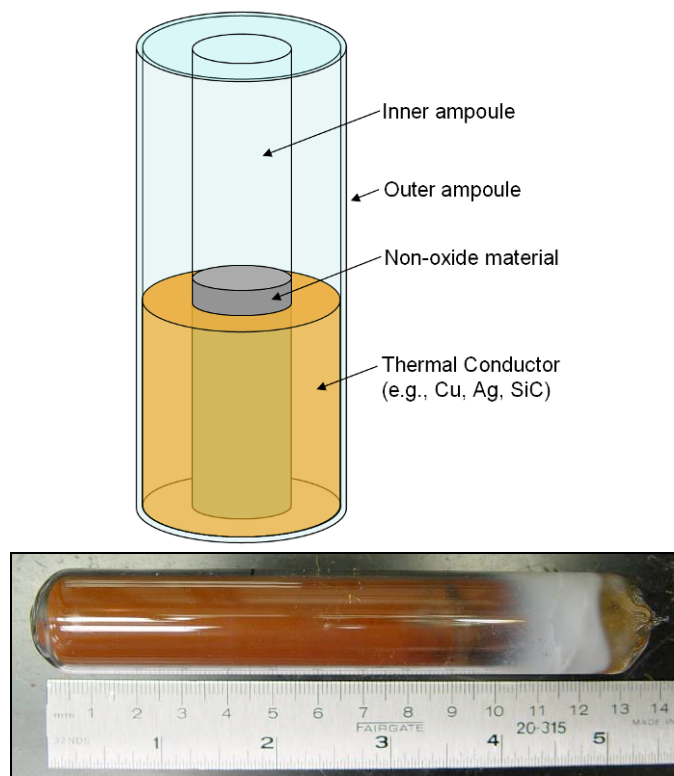


**Figure 1.** Top: double containment schematic; Bottom: double containment ampoule with copper.

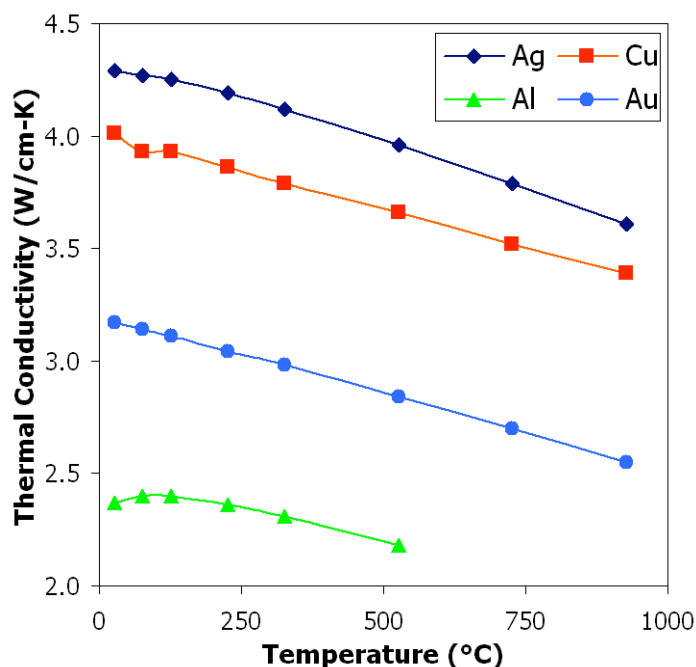


Figure 2. Thermal conductivity of different metals (Lide 2007).

## 2.2 Liquid gallium quenched single-walled ampoules

The other method developed to form bulk crack-free ingots of Cd-Ge-As glass was by quenching the ampoules in liquid gallium. A single walled ampoule was used for this process. The motivation for using this technique was based on previous reports by Hruby et al. where they recommended it as a means to quench large (e.g., 1.0-cm diameter) ingots without fracturing the CdAs<sub>2</sub> glass [4]. The primary benefit of the technique is that it allows the ingots to be quenched in a high temperature liquid so as to minimize thermal shock and cracking of the ingot. We chose to test this approach to see if we could obtain similar success with quenching 1.0-cm-diameter amorphous, crack-free ingots of CdGeAs<sub>2</sub>. Figure 3 is a picture of the setup. The details of the proposed quench process are as follows:

- 1) Heat and rock the melt at 800°C for 24 h.
- 2) Cool the ampoule inside the furnace at 5°C/min to ~ 650°C.
- 3) Heat the gallium bath to 150° to 200°C.
- 3) Quickly remove the ampoule from the furnace, and quench it in the gallium bath.
- 4) Allow the ampoule to soak/anneal in the Ga bath for several hours.
- 5) Remove the ampoule from the Ga bath and anneal it near the glass transition temperature to remove thermal stresses.



**Figure 3.** Liquid gallium in an alumina crucible at  $\sim 150^\circ\text{C}$ .

### 2.3 New Chemistries

In addition to Cd-Ge-As glass, other amorphous semiconductors were also made from the chalcogenide family. There are three primary reasons for choosing this material system. Chalcogenide glasses are known to be very sensitive to optical photons, and they have many properties that can be manipulated via exposure to sub-band-gap illumination. This material also has physical properties that match the previously stated boundary conditions for a good gamma detector (moderate to high  $Z$ , moderate bandgap, and high resistivity). And thirdly, from a processing point of view, chalcogenide glasses are superior glass formers, and are significantly easier to work with than the fragile glasses from the chalcopyrite system. Two compounds in particular were chosen,  $\text{As}_2\text{Se}_3$  and  $\text{As}_{40}\text{Se}_{48}\text{Te}_{12}$ . The composition of the ternary compound was selected based an extensive survey of publish properties [7-9]. The design goal was to simultaneously optimize density and resistivity. The addition of Te to As-Se glasses has the effect of increasing density, but decreasing resistivity, Figure 4. The composition chosen provided a comfortable compromise between those objectives.

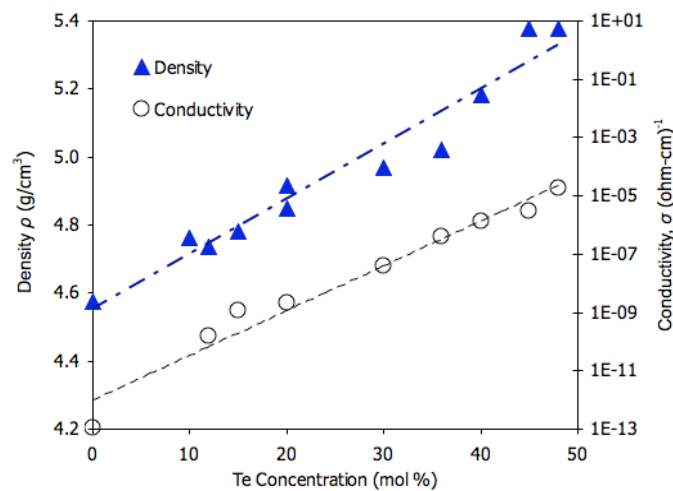


**Figure 4.** Plot of density and conductivity as a function of Te concentration for  $\text{As}_{40}\text{Se}_{(60-X)}\text{Te}_X$  [7,8].

## 2.4 Processing Summary

With two different processing methods for synthesizing bulk amorphous Cd-Ge-As glass, and four different compositions (Ge = 0.45, 0.65, 0.85, and 1.0), there was the opportunity to investigate processing-property and composition-property correlations. Since one of the liabilities of amorphous semiconductors is the high density of defect states near the band edge, the initial point of optimization was the goal of reducing the density of those defect states. Selected ampoules were back-filled with Ar-H gas blend with the goal to use hydrogen to passivate dangling bonds in the material. Optical spectroscopy was used to measure the absorption coefficient, which is an indication of defect density at the band edge. Figure 5 shows the results of comparing the effects of Ge content, quench method, and the use of H as a passivating dopant. Absorption curves with lower absolute values and a steeper approach to the band edge indicate a lower density of defect states near the band gap.

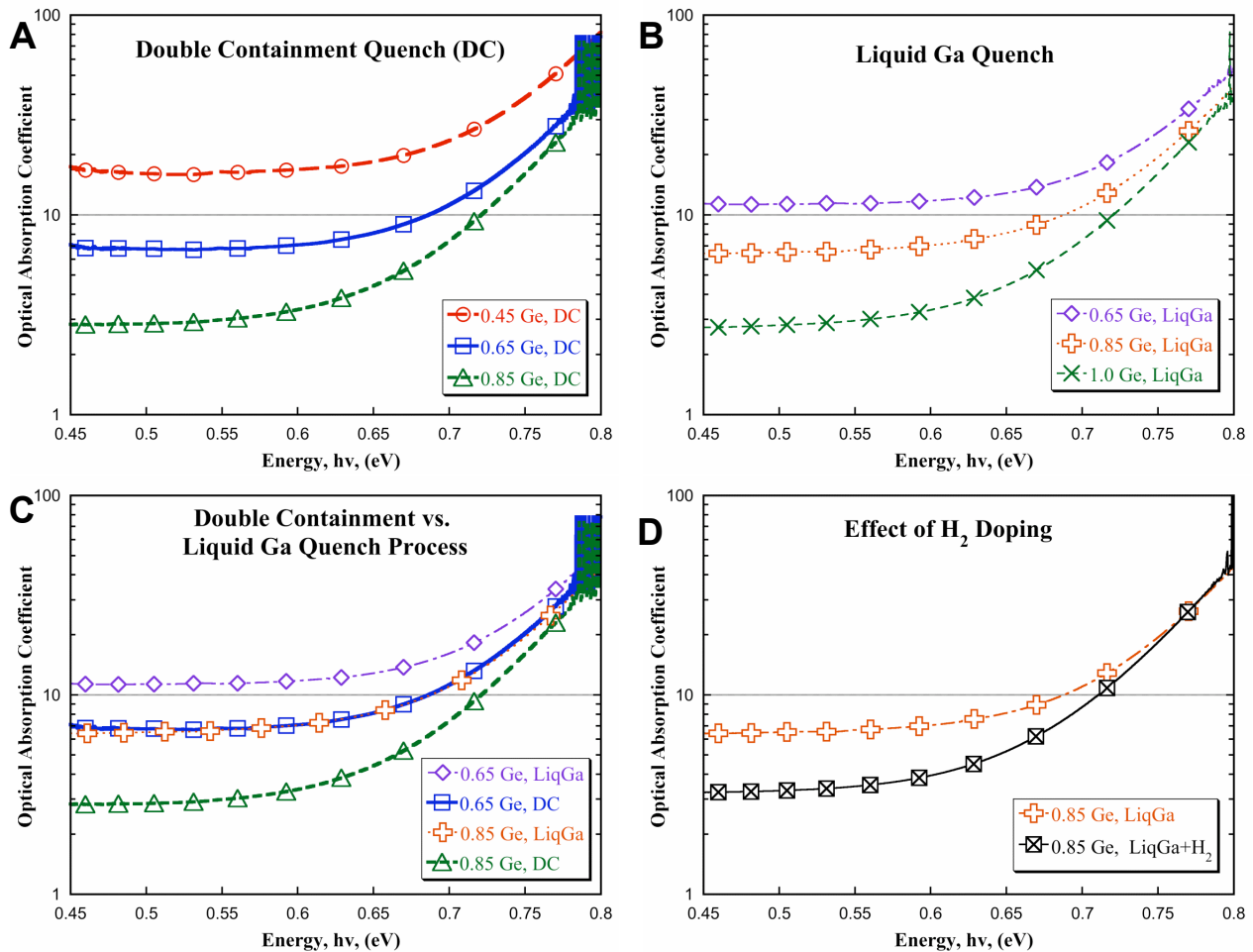


**Figure 5.** Optical absorption coefficient plots as a function of photon energy for CdGe<sub>x</sub>As<sub>2</sub> glass. (A) double-containment (DC) quench method; (B) liquid Ga quench method; (C) DC vs. liquid Ga quench method; (D) effect of H<sub>2</sub> doping for samples made via liquid Ga quench process.

The following is a summary of the results:

1. Increased Ge content results in lower optical absorption (Figure 5 A and B)
2. Water quenching with a double-containment vessel results in lower optical absorption (Figure 5 C)

3. Hydrogen doping was effective in reducing the amount of optical absorption (Figure 5 D)

In summary, then, the optimum processing path for synthesizing bulk amorphous Cd-Ge-As glass would involve higher Ge content glasses doped with H, processed in a double-containment vessel and quenched in water. The intent is to use this processing strategy to synthesize Cd-Ge-As glasses for the remainder of the project. A list of specimens synthesized this fiscal 2007 is shown in Table 2.1.

**Table 2.1.** Summary of ampoules produced in FY07

ID	Laboratory Book No.	Composition
ASGRAD-31	BNW59200-069	$Cd_{1.00}Ge_{0.65}As_{2.00}$
ASGRAD-32	BNW59200-072	$Cd_{1.00}Ge_{1.00}As_{2.00}$
ASGRAD-33	BNW59200-074	$Cd_{1.00}Ge_{0.85}As_{2.00}$
ASGRAD-34	BNW59200-075	$Cd_{1.00}Ge_{0.65}As_{2.00}$
ASGRAD-35	BNW59200-076	$Cd_{1.00}Ge_{1.00}As_{2.00}$
ASGRAD-36	BNW59200-078	$Cd_{1.00}Ge_{0.65}As_{2.00}$
ASGRAD-37	BNW59200-079	$Cd_{1.00}Ge_{1.00}As_{2.00}$
ASGRAD-38	BNW59200-082	$Cd_{1.00}Ge_{0.85}As_{2.00}$
ASGRAD-39	BNW59200-084	$Cd_{1.00}Ge_{0.65}As_{2.00}$
ASGRAD-40	BNW59200-086	$Cd_{1.00}Ge_{0.85}As_{2.00}$
ASGRAD-41	BNW59200-087	$Cd_{1.00}Ge_{0.85}As_{2.00}$
ASGRAD-42	BNW59200-090	$Cd_{1.00}Ge_{0.85}As_{2.00}$
ASGRAD-43	BNW59200-091	$Cd_{1.00}Ge_{0.65}As_{2.00}$
ASGRAD-44	BNW59200-092	80mol% $Cd_{1.00}Ge_{0.45}As_{2.00}$ 20mol% $Ag_{1.00}Ga_{1.00}Te_{2.00}$
ASGRAD-45	BNW59200-096	$Ag_{1.00}Ga_{1.00}Te_{2.00}$
ASGRAD-46	BNW59200-097	$Cd_{0.45}Te_{0.45}As_{0.05}Ag_{0.05}$
ASGRAD-47	BNW59200-098	$(Cd_{0.885}Zn_{0.115})-(Ge_{0.70}Si_{0.30})-As_{2.00}$
ASGRAD-48	BNW59200-102	$Cd_{1.00}Ge_{0.45}As_{2.00}$
ASGRAD-49	BNW59200-103	$Cd_{1.00}Ge_{1.00}As_{2.00}$
ASGRAD-50	BNW59200-104	$Cd_{1.00}Ge_{1.00}As_{2.00}$
ASGRAD-51	BNW59200-105	$Cd_{1.00}Ge_{0.65}As_{2.00}$
ASGRAD-52	BNW59200-107	$As_{40}Se_{48}Te_{12}$
ASGRAD-53	BNW59200-108	$Cd_{1.00}Ge_{0.45}As_{2.00}$
ASGRAD-54	BNW59200-109	$As_{40}Se_{60}$
ASGRAD-55	BNW59200-110	$Cd_{1.00}Ge_{0.45}As_{2.00}$
ASGRAD-56	BNW59200-111	$Cd_{1.00}Ge_{0.65}As_{2.00}$
ASGRAD-57	BNW59200-112	$Cd_{1.00}Ge_{0.45}As_{2.00}$
ASGRAD-58	BNW59200-113	$Cd_{1.00}Ge_{0.15}As_{2.00}$
ASGRAD-59	BNW59200-114	$As_{40}Se_{48}Te_{12}$

### 3.0 Discovery of New Metastable Phase

During one of the experiments, an ingot partially crystallized during quenching. Close examination revealed that it was a mixture of different crystalline phases in an amorphous matrix. X-ray diffraction analysis determined that one of the phases was  $\text{CdGeAs}_2$ , while the other was unknown. Since the crystals formed during the quenching process, the unknown phase was suspected to be metastable. Examination of thermal analysis data collected by ourselves and others [10] shows the presence of metastable phases. The material was subsequently analyzed using SEM EDS to determine the stoichiometry, electron-back-scattered diffraction (EBSD) to determine crystallographic orientations, and various other techniques (Figure 6). Reitveldt analysis of the unknown metastable phase is in progress to determine its exact crystal structure. The results were that the blue matrix in Figure 6A was amorphous, the multi-colored region in the center was a cluster of  $\text{CdGeAs}_2$  crystals, and the long rod shaped features coming from the edge of the micrograph toward the center was the new metastable phase.

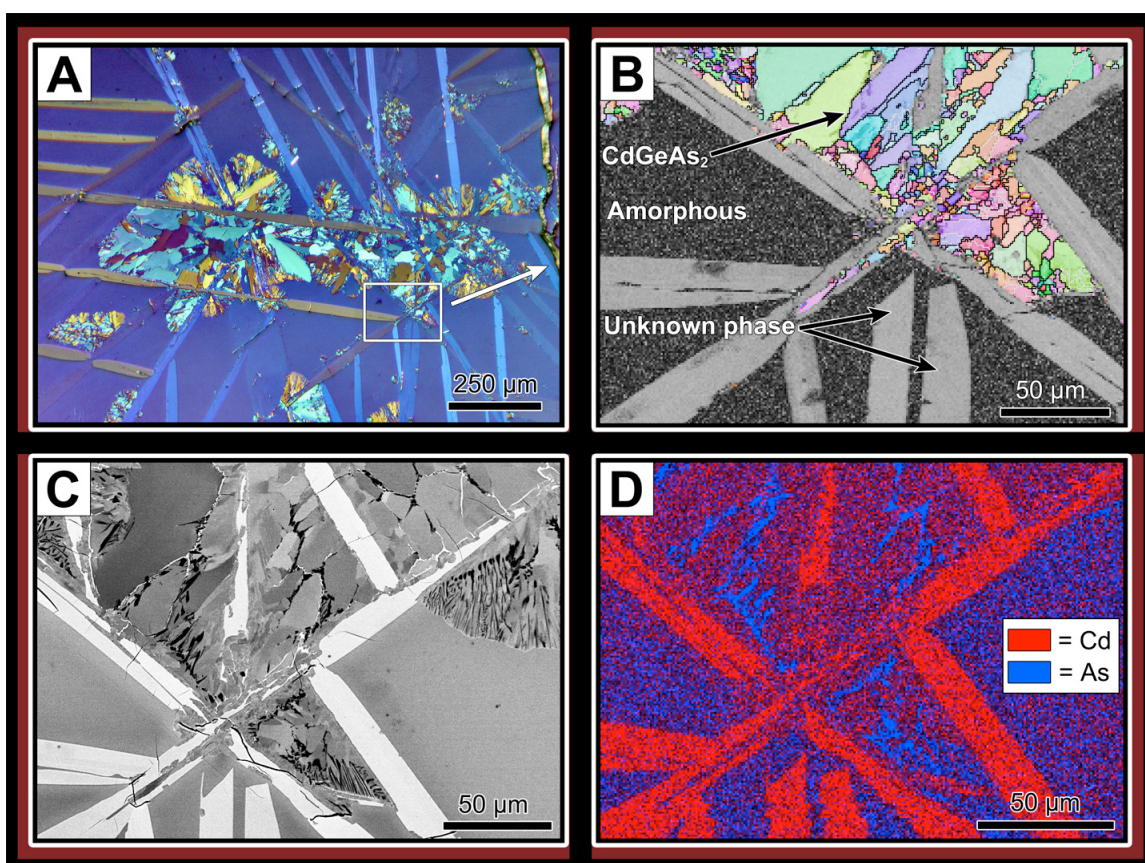


**Figure 6.** Microscopic analysis of metastable phases formed in Cd-Ge-As during quenching. Polarized reflected light microscopy (A) revealed two distinct crystal morphologies (polycrystals and needles) in an amorphous matrix. Examination by XRD detected  $\text{CdGeAs}_2$  and a new, unidentified phase(s). Electron backscattered diffraction (B) determined the polycrystals (colored) were  $\text{CdGeAs}_2$ , and confirmed the matrix was amorphous, but diffraction patterns from needles were unidentifiable. Compositional differences ( $Z_{\text{ave}}$  contrast) were accentuated using SEM BSE (C), and stoichiometry was determined by quantitative EDS mapping (D, polycrystals =  $\text{CdGeAs}_2$ , needles =  $\text{Cd}_3\text{Ge}_2\text{As}_4$ ). Lattice parameters, space group, and structure factor calculations for the new phase are in progress<sup>1</sup>.

<sup>1</sup> Winner of Best Poster Competition at the Materials Science & Technology (MS&T2007), Detroit, MI, October, 2007.

## 4.0 Radiation Response Testing: Sealed Alpha Sources

Alpha particles provide a convenient way to characterize the performance of a detector for several different reasons. First, they provide a 100% probability of interaction; second, each particle deposits 100% of its energy, enabling an accurate calculation of total flux; third, the location where the energy was deposited can be known, thus enabling computation of charge transport properties; and fourth, the influence of the radiation can be easily controlled or turned “on and off” using a simple shutter. Because of these experimental testing advantages, sealed alpha sources were chosen as a starting point for materials characterization.

### 4.1 Current-voltage curves

The first set of experiments performed involved measuring the current voltage characteristics of a specimen with and without exposure to an alpha source. Several different experiments were done with three different materials, one was a Cd-Ge-As glass, and the other two were As-Se-Te glasses. Figure 7 shows the current-voltage curve for  $\text{CdGe}_{0.85}\text{As}_2$  sample at  $-40^\circ\text{C}$  over 0-100V. The change in current vs. voltage curve with and without exposure to the sealed source was pronounced – an increase of 36.4 nA.

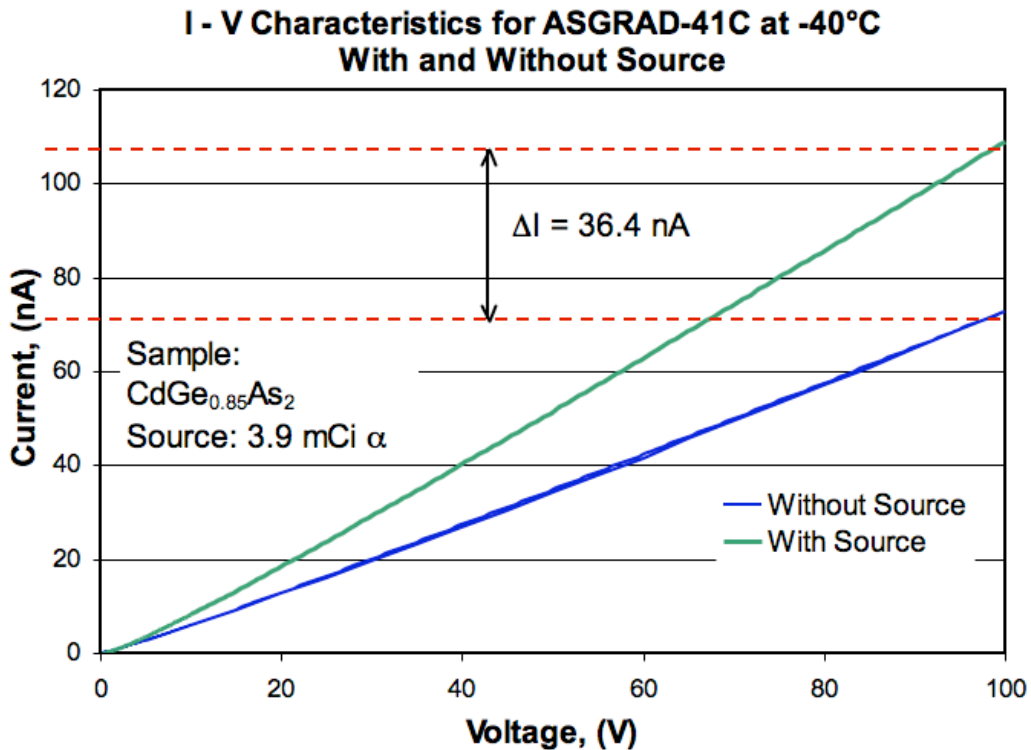
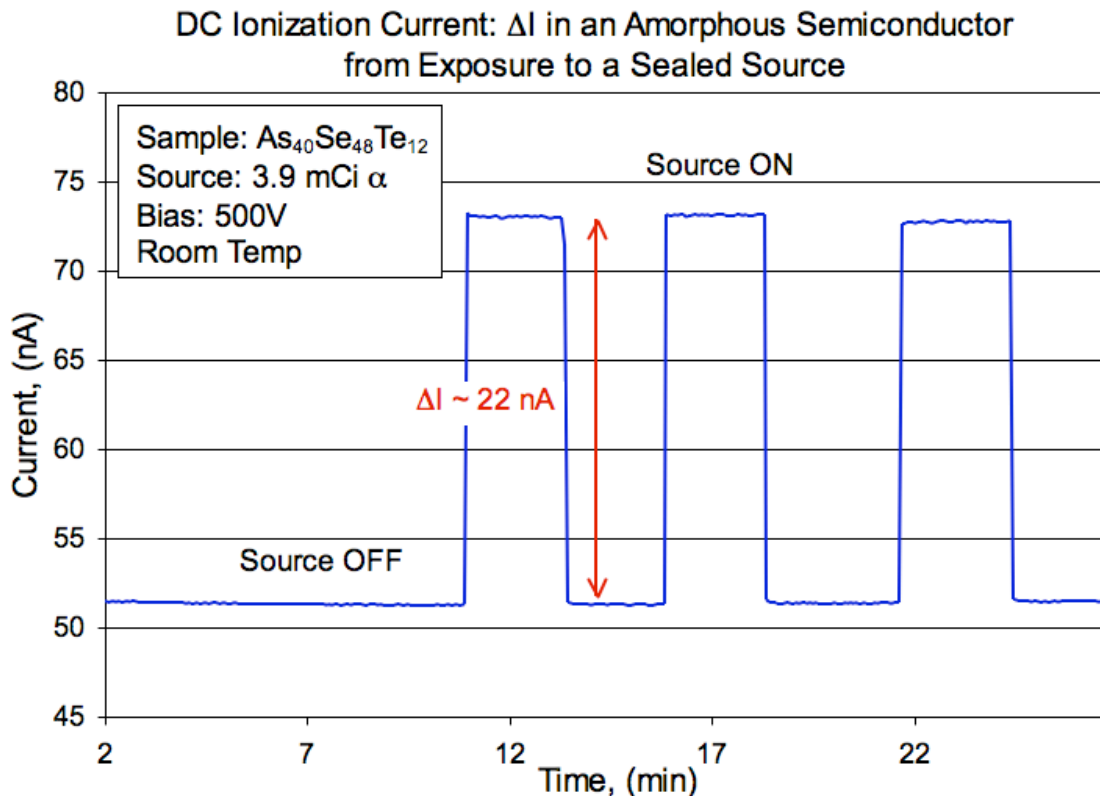


Figure 7. Current-voltage curve for  $\text{CdGe}_{0.85}\text{As}_2$  from 0-100 V at  $-40^\circ\text{C}$

## 4.2 DC ionization experiments

The next set of experiments involved measuring the transient response for exposure to alpha radiation. Direct current ionization tests were done on two different chalcogenide amorphous semiconductors at room temperature. The specimens were slowly biased up to a high voltage ( $\geq 500\text{V}$ ), and a sealed alpha source (secured to a pivoting platform above the sample) was rotated over the top of and alternately away from the specimen. When the sealed source was over the specimen, there was a rapid increase in the measured current, almost instantaneously, that essentially reached a plateau value. After waiting for a couple of minutes, the sealed source was rotated away from the specimen, and the current again almost instantaneously decreased back to its base-line value. This test was repeated several times, thus forming a square wave function. A plot of the data for  $\text{As}_{40}\text{Se}_{48}\text{Te}_{12}$  is shown in Figure 8. The data shows that the high bias applied to the sample was able to fill most if not all of the trap states such that when exposed to ionizing radiation, the sample became significantly more conductive, as the increase in ionization induced electron hole pairs traversed across the sample. When the ionizing radiation was removed, the population of electron hole pairs was reduced, and the conductivity rapidly returned to its base line value. The three cycles show practically no drift in the base line current level or any evidence of hysteresis. Evidence of incomplete trap state filling would have resulted in a waveform that was not square, but rather with a curved rise time and a curved decay. The ability to fully populate trap states is an important step in improving charge carrier mobility.



**Figure 8.** Current vs. time for  $\text{As}_{40}\text{Se}_{48}\text{Te}_{12}$  as a function of exposure to a sealed source at room temperature and a bias of 500V.

Additional experiments were done to evaluate the variation in DC ionization current as a function of applied field. These tests were done with an amorphous specimen of  $\text{As}_2\text{Se}_3$ . The results in Figure 9 show that as the field increased, the DC ionization current also increased. This response holds promise that improved performance with this material may be possible by using higher biases.

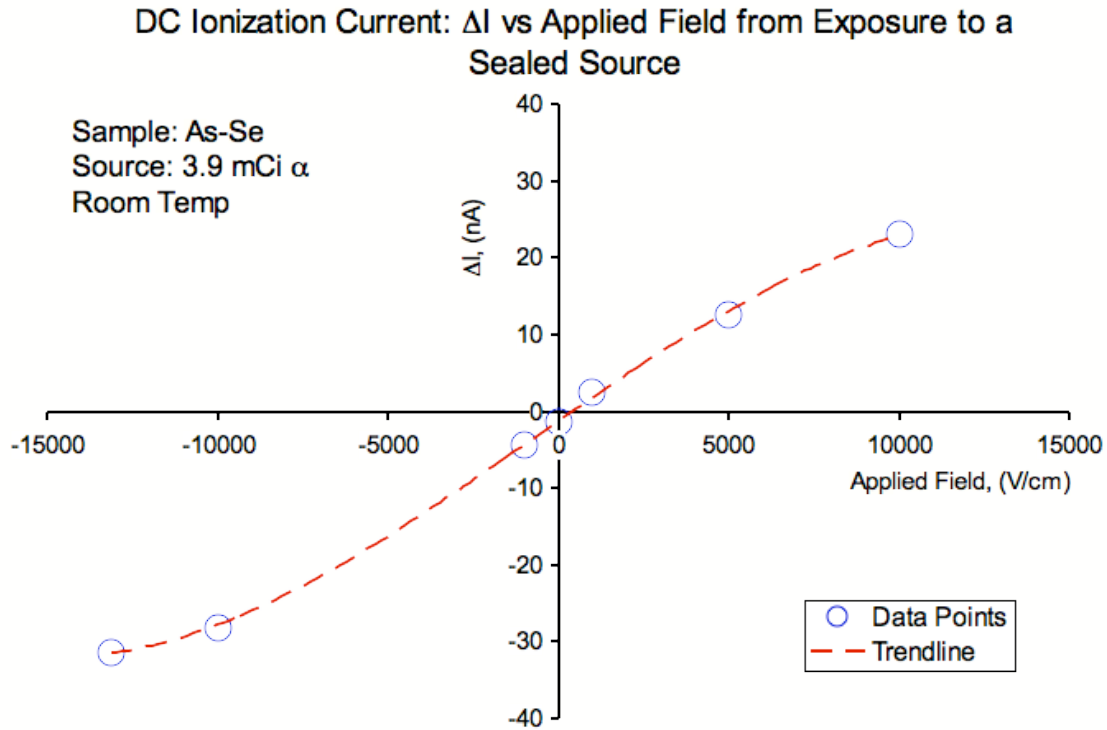


**Figure 9.** Variation in DC ionization current as a function of applied field.

Because the specimen was exposed to alpha radiation from a source with known activity and the sample testing geometry was known, the amount of energy deposited into the specimen could be calculated by taking into account various attenuation factors. The energy coming out of the sample could be directly computed from the measured DC ionization current ( $\Delta I$  due to exposure to the source) and the applied bias voltage. A ratio of the power output (bias voltage times measured ionization current) divided by the energy of the radiation deposited per second (energy per alpha particle times flux) was then computed, and the results are shown in Figure 10. The data shows that the measured signal response under a constant amount of radiation exposure increases in an exponential fashion with increasing bias voltage. For this experiment, the charge carrier losses due to trapping phenomena were compensated for at a bias of approximately 7000 V/cm. At higher bias voltages, the signal power (bias voltage times measured current) exceeded the rate of energy deposition on the sample by sealed source. This clearly demonstrates that a signal gain or amplification can be achieved in this material. This implies that the material can be used as a solid state photomultiplier, and can be tuned to create a gain in signal strength greater than the energy deposited by the incident radiation. The explanation of this phenomenon is as follows:

- 1) The incident radiation ionizes the active material to form electron-hole (e-h) pairs.
- 2) The e-h pairs are accelerated by the applied bias field towards the contact surfaces.
- 3) As the charge carriers travel through the material, they collide with and are scattered by local structural defects in the amorphous material.

- 4) If the charge carriers have been accelerated by the bias voltage to a sufficient energy, they will create additional e-h pairs through these collisions and scattering events.
- 5) At sufficiently high bias voltages, these newly-formed scattered charge carriers will also be accelerated to a sufficient kinetic energy so as to produce tertiary charge carriers when they scatter.
- 6) The net result is a cascading or avalanche effect.

As such, these materials maybe suitable for use in applications as photodiodes coupled to scintillator detectors. These same results were reproduced with  $\text{As}_{40}\text{Se}_{60}$  glass for different configurations of contacts and electrodes.

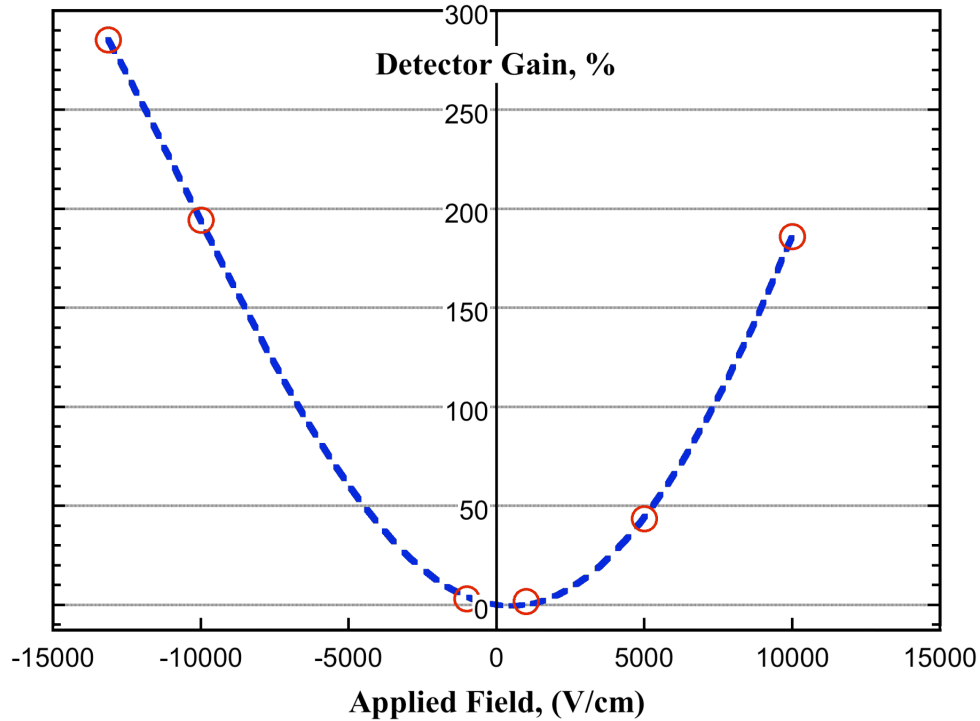


**Figure 10.** Detector gain as a function of applied field for amorphous  $\text{As}_2\text{S}_3$  for exposure to a sealed alpha source.

### 4.3 Summary

Overall, we have demonstrated that measuring DC ionization conductivity is a viable experimental method of screening of glasses for their potential application as gamma detectors. By cooling Cd-Ge-As glass, we were able to demonstrate measurable radiation sensitivity by comparing I-V curves collected with and without exposure to alpha radiation. The room temperature transient response to radiation was studied by measuring the DC ionization current with  $\text{As}_{40}\text{Se}_{48}\text{Te}_{12}$ . The sharp step changes between source on and off conditions indicates that the high bias may be sufficient to fill trap states such that ionized electron hole pairs are able to move across the material with higher mobility. The effect of varying applied field on DC ionization current measurements was studied using  $\text{As}_{40}\text{S}_{60}$ . The data demonstrates that not only is it possible to compensate for charge trapping losses, but that actual signal

gain can be attained by operating at high biases. Thus, in spite of the short-range order and trapping issues, these amorphous semiconductors show a measurable response upon exposure to ionizing radiation, and thus show promise for application as radiation detector materials for either direct detection of radiation or as photodiodes coupled to scintillators.

## 5.0 Collaboration with the University of Illinois at Urbana-Champaign (UIUC)

As in the first year of the project, collaboration with the University of Illinois at Urbana-Champaign (UIUC) was continued. Our principal collaborator is Prof. Angus Rockett and his group. During this year measurements carried out at UIUC on this project have included electrical measurements including Hall-effect, four point probe resistivity, and current/voltage; micro chemical measurements including x-ray diffraction, secondary ion mass spectrometry (SIMS), photoelectron spectroscopy; and optical characterization by transmission and reflection and by ellipsometry. Some devices and contacts have also been produced on the materials.

### 5.1 Samples analyzed

The samples studied at UIUC and analyzed as discussed in the later sections are listed in Table 5.1. A summary of the analyses applied to each sample and/or representative results are provided in the table. These analyses directly supported our material development and process improvement efforts.

**Table 5.1** Samples analyzed at UIUC and analysis results summary.

Lab Book No.	[Ge]	Quench Method <sup>1</sup>	XRD	Resistivity			Chemical		Optical	
				Hall vdP ohm-cm	UIUC 4 Pt ohm-cm	PNNL ohm-cm	XPS/UPS	SIMS	T/R	Ellipsometry
59200-023B	1.0	H <sub>2</sub> O	Poly		9.50E-03			Yes		Yes
59200-048A	1.0	H <sub>2</sub> O			1.35E+07					
59200-056B	0.45	DC H <sub>2</sub> O	Amo	4.82E+07	7.50E+06	4.65E+05		Yes	Yes	Yes
59200-058	0.24	H <sub>2</sub> O	Amo	1.97E+06	7.00E+07				Yes	Yes
59200-065	0.85	DC H <sub>2</sub> O	Amo	9.20E+06	8.35E+07			Yes	Yes	Yes
59200-065	0.85	DC H <sub>2</sub> O	Poly		3.45E+07				Yes	
	0.65	DC H <sub>2</sub> O	Amo		6.20E+07				Yes	
59200-068	1.0	DC H <sub>2</sub> O	Poly		1.45E-03			Yes	Yes	Yes
59200-069	0.65	L. Ga	Amo		2.50E+07				Yes	
59200-	0.85	L. Ga	Amo	1.77E+06	3.75E+07		Yes		Yes	Yes
59200-076	1.0	L. Ga	Amo	2.00E+06	5.05E+07				Yes	Yes
59200-078	0.65	L. Ga	Poly		4.60E+07				Yes	
59200-087	0.85	L. Ga	Amo	1.51E+06	3.50E+07	1.77E+06			Yes	Yes
59200-087	0.85	L. Ga		1.00E+06	3.35E+07				Yes	
59200-087	0.85	L. Ga			3.35E+07				Yes	Yes

<sup>1</sup> H<sub>2</sub>O = water quenched;

DC H<sub>2</sub>O = water quenched double containment ampoule;

L. Ga = Liquid gallium quenched ampoule

### 5.2 Electrical measurements

To provide contacts for Cd-Ge-As (CGA) electronic property characterizations and for some devices, ohmic contacts are necessary. We have established that most high-work function metals such as Au, Ag, and Ti show good ohmic behavior. The relatively lower work function Al did not generally provide good

ohmic contacts (see discussion of Schottky contacts, below). Resistances from contact to contact are linear and reflect the resistivity of the CGA material.

All polycrystalline CGA showed low resistance in the range of tens of ohms across the ~5 mm distance between contacts in samples ~2 mm thick, while amorphous materials show much higher resistances through samples of the same dimensions, of the order of  $10^8$  ohms (Figure 11) as expected from the literature. Thus, the amorphous materials show resistances approximately  $10^7$  larger than the crystalline materials. It is worth noting that the data for the amorphous materials is much noisier than for the polycrystals. This is attributed to the low signal values that accompany these higher resistivity materials.

Van der Pauw and four-point probe measurements should exclude contact resistances from the values determined. Sample resistivity values measured for all samples tested are given in Table 5.1 **Samples analyzed at UIUC and analysis results summary.** Values for a given type of measurement were relatively reproducible but, as is clear from

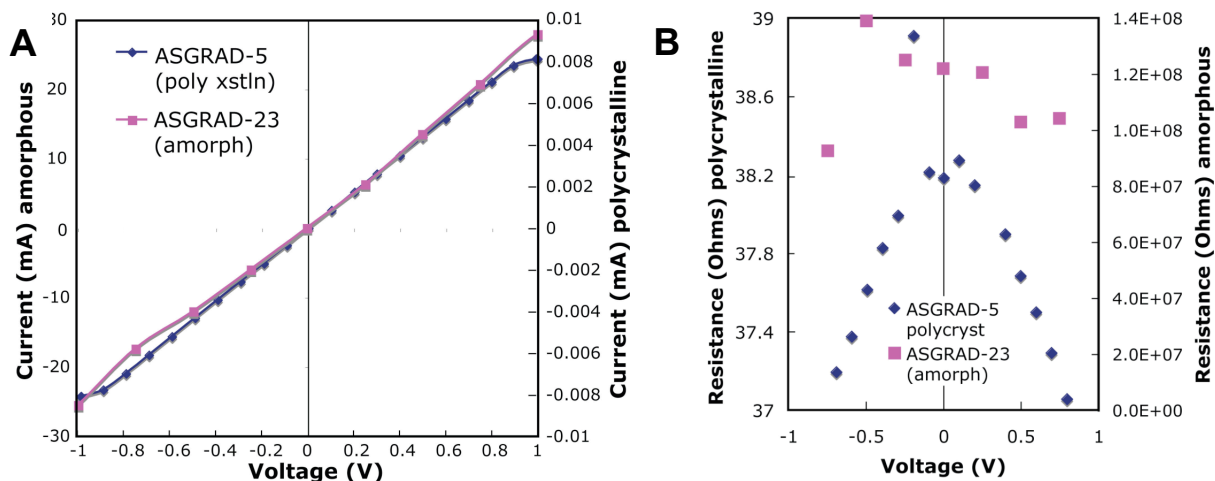


**Figure 11.** (A) Current-voltage measurements contact to contact across two samples, polycrystalline ASGRAD 5 and amorphous ASGRAD 23. (B) The resistances calculated as a function of voltage from the data in (A)

Table 5.1 **Samples analyzed at UIUC and analysis results summary.**, different measurements yielded significantly different values. A comparison of the individual contact pairs used in the measurements showed that the resistivity of some samples was asymmetric, being consistently greater in one direction than another. In one case, the ratio of the resistivity in the two orientations was a reproducible  $2.7 \pm 0.2$ .

The variability of the van der Pauw measurements suggested that an alternate technique to measure resistivities would be in order. Resistivities were therefore also measured near room temperature by four point probe. The values measured by four point probe were generally ~20 times higher than from the van der Pauw measurements but the difference was not consistent and one four point measurement was lower than the van der Pauw value. Four point probe measurements were also conducted at PNNL for two samples with results that were consistent with the van der Pauw sample in one case but significantly lower than the van der Pauw value in the other case. The latter sample was the same one that had the higher resistivity in the UIUC four point probe. We conclude that making contact to this sample (ASGRAD 23) may have been difficult for some reason. In spite of the variations in resistivity for the

various methods, the temperature dependences showed similar activation energies for most samples in the range of  $0.5 \pm 0.2$  eV, consistent with the observed optical energy gap of the material (see below).

### 5.3 Optical measurements

Most samples were measured by transmission and reflectance in a Cary spectrophotometer. Typical results show modest transmission of 10-50% at long wavelengths and with absorption rising exponentially near an apparent band edge until no detectable transmission occurred. A number of samples were mechanically polished to thin the material as much as practical to obtain greater transmission but no significant differences in the data were obtained. The combination of transmission and reflection data was converted to absorption coefficients and examples of these are shown in Figure 12. Numerical modeling of the absorption data showed exponential band tails with widths (Urbach energies) on the order of  $60 \pm 25$  meV.

The samples measured to longer wavelengths show a minimum absorption coefficient on the order of  $2\text{--}20 \text{ cm}^{-1}$  ( $0.2\text{--}2 \text{ mm}^{-1}$ ). This is suggestive of a high level of midgap states spread across the energy gap of the material. The transmission/reflection data does not extend to high enough energies to get a strong indication of the energy gap of the material. That information was obtained by ellipsometry, which measures the dielectric response of the material by reflection only. Therefore the sample thickness was not a problem. Typical ellipsometry data for several samples are shown in Figure 12. The data is complementary to the transmission data because if the sample is sufficiently transmitting and absorbing no accurate ellipsometry data could be obtained.

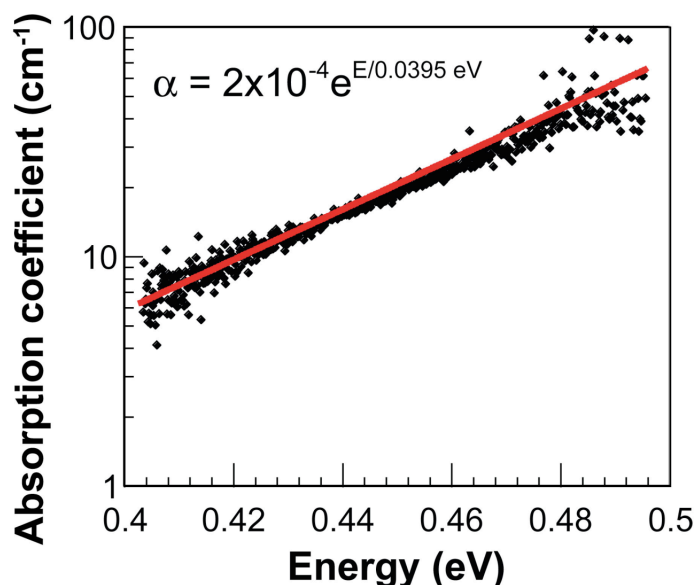


**Figure 12.** Typical optical transmission/ reflection data results for sample ASGRAD 23.

The ellipsometry data show broad absorption edges. The energy gaps obtained in this way are significantly higher than those obtained from electrical data, but were consistent with published values. (The difference between electrical and optical band gap measurements is often attributed to the fact that

the Fermi level is pinned in the middle of the band gap for amorphous semiconductors.) For the data in Figure 13, these energy gaps range from 0.9 to 1.2 eV. The ellipsometry data shows similar behaviors to that of a-Si:H and other amorphous semiconductors. The absorption edges are very broad and do not show a linear behavior when plotted as  $(\alpha h\nu)^2$  vs.  $h\nu$  as one would expect for free-electron bands.

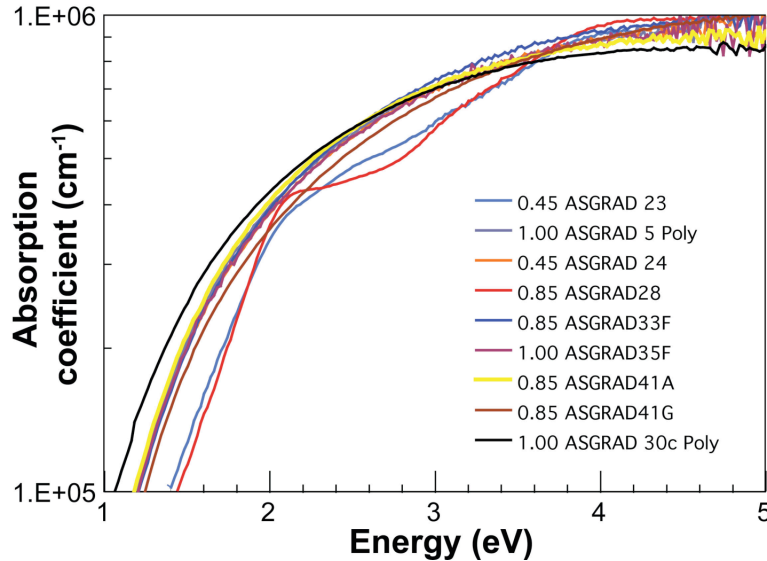


**Figure 13.** Typical ellipsometry data for several samples. The values to the left of the ASGRAD number in the legend are the Ge fraction,  $x$ , in the  $\text{CdGe}_x\text{As}_2$ .

The optical absorption coefficients derived from ellipsometry and transmission and reflection can be summarized as typical of amorphous semiconductors containing a large number of midgap states. The shifts in the absorption edges based on ellipsometry vary more based on processing conditions than on composition. For example, the largest band gaps correspond to samples ASGRAD-23 and ASGRAD-28 which were processed using the DC quench method, whereas ASGRAD-33 and 35 were processed using the liquid Ga quench method. Within each process method, the higher Ge content specimens had slightly higher band gaps. Two samples (28 and 23) show sharper and more exponential edges. These samples also show evidence of a variable absorption behavior with wavelength. This could be due to Fresnel cavity effects but the wavelength behavior is not correct. The behavior could also result from finer structure of the density of states at the band edge. Further analysis will need to be done to determine if these features are significant.

## 5.4 X-ray diffraction

The variability in optical and electrical data could reflect differences in the microstructure of the samples. It is clear that polycrystalline material is highly conductive even though the optical data shows clear evidence of an energy gap, based on the ellipsometry data. It is therefore of interest to characterize the structure in more detail.

The structures of the samples were studied by x-ray diffraction to determine if there was any detectable difference in pair-correlation function for the amorphous materials and to detect any correlations with observed properties. Example data is shown in Figure 14. Similar spectra were obtained from the other amorphous materials studied.

Some of the observations that may be made based on the x-ray data are as follows. (1) There was no significant difference in peak shape or position from one amorphous sample to another. The greatest differences were in the relative intensities of broad peaks around  $45^\circ$  and  $51^\circ$ . A change in peak position would correlate with a difference in average interatomic distance. All peaks centered at  $28.2^\circ$  occur at the same positions and have virtually identical widths (correlated with domain size). All peaks at  $79^\circ$  occur at the same positions. Therefore the basic first, second, etc. nearest neighbor distances are unchanged from sample to sample. (2) The polycrystalline samples show sharp peaks at different positions from the amorphous material. Note, for example, the position of polycrystalline peak positions for sample ASGRAD 36 and ASGRAD 5 in Figure 14. A similar difference was observed in the polycrystalline sample, ASGRAD 30. The differences indicate that the polycrystalline materials may contain a mixture of phases with different crystal structures, which is reasonable considering the metastable phase that was discovered and discussed in Section 3.0. (3) The peaks for polycrystals do not occur at the same locations as for the amorphous peaks (especially at the higher angles), indicating that there is a difference in interatomic spacing between the two materials. This is also to be expected, considering that the amorphous phase is more dense than the crystalline phase, thus the nearest neighbor correlations (high angles) occur at shorter d-spacings (larger 2 theta values) for the amorphous materials than for their crystalline counterparts.

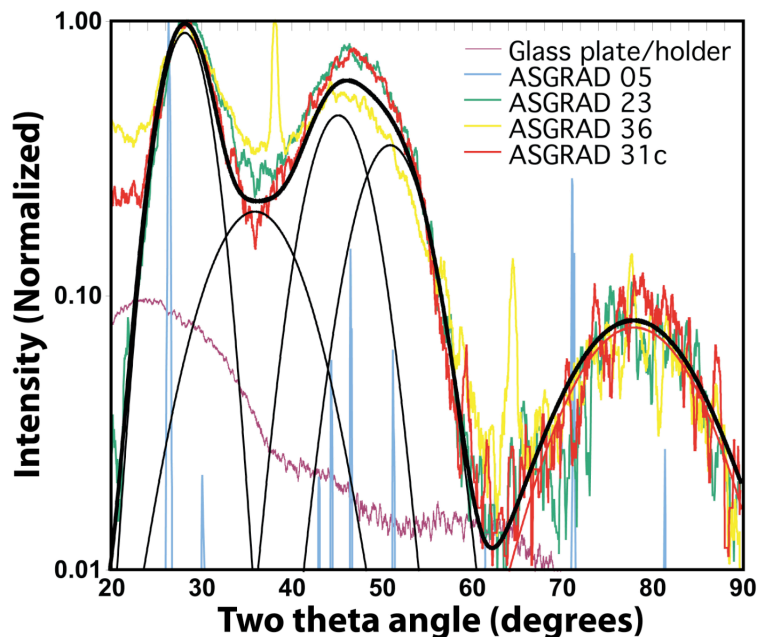


**Figure 14.** X-ray diffraction data for four samples including one polycrystalline sample (light blue), one partially crystalline (yellow), and two amorphous (ASGRAD 23 and ASGRAD 31c). Each data set was fit with a series of Gaussian curves (black). The fit example was for the ASGRAD 31c. Spectrum for the glass specimen holder is included as evidence that the instrument did not contribute to the data.

## 5.5 Microchemistry

The absence of a measurable structural difference between the different amorphous samples indicates that the differences in electrical and optical properties are not the result of medium to long-range structural differences. We therefore considered chemical differences both by secondary ion mass spectrometry

(SIMS) and photoelectron spectroscopy (PES). SIMS analysis was carried out on four samples in a Cameca IMS-5f instrument using an  $O_2$  ion beam. This analysis condition is highly sensitive to electropositive species and to a broad range of transition and other metals. All samples showed modest contamination with K. Some samples also showed traces of Al. In general the samples were extremely clean with almost no impurities in the bulk of the specimens. The major exception was sample ASGRAD 5, a polycrystal that showed relatively large amounts of impurity species, especially K, Ca, and Al. All samples showed a modified surface layer, apparently consisting of a surface oxide and other contamination.

Measurement of the photoelectron spectrum on one sample (ASGRAD 30) showed the presence of a wide range of peaks consistent with surface contamination. However, once the sample was briefly sputtered it showed a clean spectrum consistent with  $CdGe_xAs_2$ .

The valence band of the CGA sample ASGRAD 30 was also measured using a He lamp. The HeI photon energy is 21.2 eV, while the HeII energy is 40.8 eV. The two photon energies yield different cross-sections for interaction with valence electrons.

A typical interpretation of the valence band spectrum would place the band edge relative to the Fermi energy by fitting the data plotted on a linear scale (Figure 15 left) and extrapolating to zero signal. For the data obtained on this sample, the band edge would be at  $\sim 2.8$  eV. Because the Fermi energy should be within the energy gap, this would imply at least a 2.8 eV energy gap.

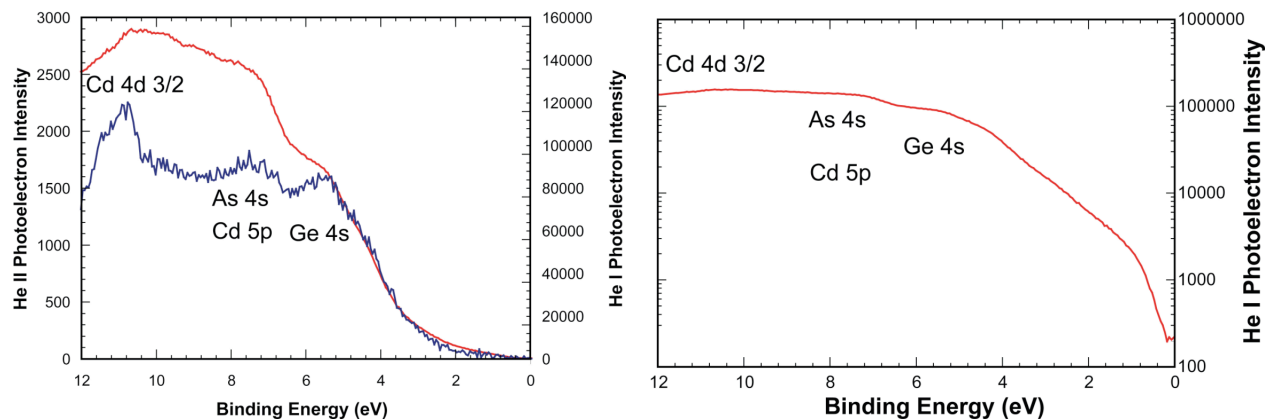


**Figure 15.** (Left) The valence band of ASGRAD 30 measured with HeI and HeII photons. The valence states likely responsible for the major transitions are labeled. (Right) Same HeI valence band spectrum as on Left, but plotted on a logarithmic scale showing the states near the Fermi energy

Plotting the HeI data on a logarithmic scale (Figure 15, Right) shows two regimes that are consistent with an exponential decrease in the density of states of the valence band. One of these regimes begins at  $\sim 3.4$  eV and continues at a moderate slow (more gradual decay of the states). This slope transitions to a more rapid decay around  $\sim 0.8$  eV and the exponential decay continues down to the background level of the measurement at  $\sim 0.3$  eV.

The photoelectron data on the valence band can now be connected to the ellipsometry and transmission data for absorption coefficient. Roughly speaking, the absorption coefficient corresponds to the photoelectron intensity. Thus, the first two decades of decrease in density of states in the valence band

corresponds to the decrease in ellipsometry data with strong absorption down to energies in the 1 eV range. The transmission data corresponds to the behavior at the bottom end of the band tail (near zero binding energy) where rapid exponential decay carries the density of states to a background level. The background level may correspond to the background count rate in the spectrometer but is more likely due to the density of states in the energy gap of the material at  $\sim 0.1\%$  of the density of states in the bulk of the valence band.

Note that the material is nominally p-type, so it would be expected that the band edge as measured by photoelectron spectroscopy would be close to the Fermi energy. In these measurements, there is a significant gap between the band edge and the Fermi energy. This suggests that either the material is n-type or that the Fermi energy is near the center of the gap.

We know from Hall effect data that the carrier type is difficult to determine in these samples. Carrier concentrations range from  $10^8$  to  $10^{12}$   $\text{cm}^{-3}$  with random variations in the sign of carrier type. Such a variation is typical of conduction dominated by defect-band conduction. In defect band semiconductors, the Fermi energy is typically near the middle of the energy gap. This is consistent with the photoelectron spectroscopy data showing a band edge close to the Fermi energy (i.e. a small energy gap) but not a clear p-type behavior. The 0.3 eV energy difference between the band tail and the Fermi energy plotted in Figure 15 (right) is close to what would be expected for a 0.6 eV energy gap semiconductor with the Fermi energy at midgap.

## 5.6 Conclusions of the materials characterization at UIUC

Based on the analyses described in this section, we conclude that the material is a typical amorphous semiconductor with a mobility gap in the range of 0.6-0.9 eV, a very broad band edge with a relatively low density of states near the mobility gap. The XRD data shows that the material has a wide range of interatomic distances. Although the structural and chemical properties are very uniform, the electrical and optical properties are not. The mobility gap and resistivity vary from sample to sample based on processing and composition variations. Difficulties in obtaining good quality electrical contacts have also introduced an additional complication. This may indicate variability in the nature of the material on the microscale sufficient to result in large variations in optical and electronic properties.

Amorphous hydrogenated Si (a-Si:H) is a typical amorphous semiconductor. The hydrogen reduces the density of states near the middle of the gap, making it much more straightforward to dope and making it a better semiconductor. Both a-Si:H and CGA glass are tetrahedrally bonded amorphous semiconductors. Thus, using a-Si:H as a model, a specimen of CGA glass was prepared with a hydrogen atmosphere in the process ampoule. The results show that when compared to a specimen of the same composition and under identical conditions, that a reduction in defect density and improved optical properties was obtained (sample ASGRAD 41, Figure 5D).

In general the conductivity of the CGA samples tested to date has been too high for room temperature radiation detection – cooling to  $-40^\circ\text{C}$  was required to sufficiently reduce the leakage current. Several approaches to improving the situation are possible. One could investigate other processing and compositional changes that could have a greater impact on reducing the density of midgap states, similar to the hydrogen experiment described above. An additional approach would be to make diode-like

(Schottky) contacts to the material. The depletion regions associated with these contacts can reduce local conductivity and provide a field to collect photocarriers generated by gamma rays.

## 5.7 Schottky contacts

We have begun investigation of the possibility of reducing the sample conductivity through contact junctions. In Section 5.2 we described how high work function metals such as Ti, Au, and Ag typically produce ohmic contacts to the CGA samples. Therefore the best potential for a high barrier Schottky contact would be to use a low work function metal. Typical examples used in organic electronic devices are Mg or Ca.

We have deposited and patterned Mg contacts on CGA samples as shown in Figure 16. The contacts were then studied by current/voltage measurements from Mg to Mg, from Mg to a Ag ohmic contact used for Hall effect measurements on the opposite side, and from Mg to a probe resting directly on the CGA.

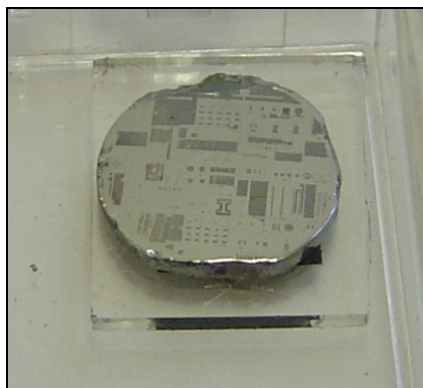


**Figure 16.** A test pattern and contact arrays of Mg metal deposited on Sample ASGRAD 41c. Current - voltage measurements were made from Mg contact to Mg contact, from Mg contact to an ohmic contact (used for Hall effect) on the back side of the wafer, and from Mg contact to a probe placed directly on an exposed area of the CGA.

The most dramatic results in measurements so far are a large photoconductive response between adjacent Schottky barrier contacts (Mg to Mg) when the sample is exposed to white light. An example of this behavior is shown in Figure 17. Upon exposure to white light, the current increased by over 2 orders of magnitude!

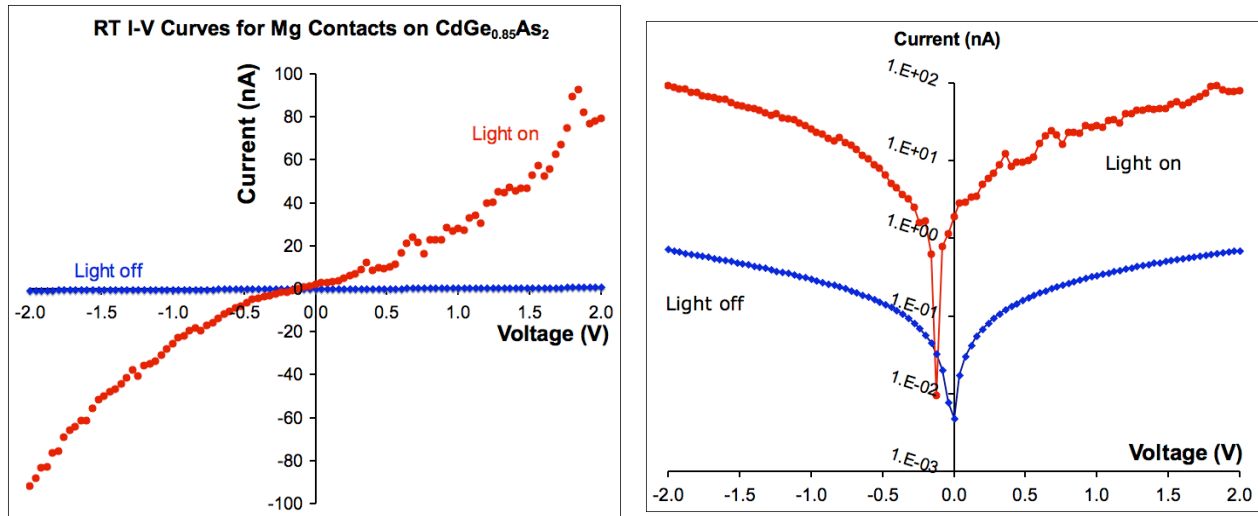


**Figure 17.** Left, a linear scale plot and right a logarithmic plot of the current/voltage curves for sample 41c measured between two sets of Mg contacts in the light and in the dark. A large difference in conductivity is observed.

***Because transient photoconductivity is precisely the expected result of a gamma-ray detection event, this result is very exciting as a possible gamma ray detector.***

The major problem with the Schottky contact study to date is the large variation in device behavior from contact to contact and the relative delicacy of the Mg contacts. The latter is easily solved by over-coating the Mg with another protective metal such as Al and/or Au. The former is more troublesome. However, if these issues can be resolved, it should be possible to build a high-performance radiation detection device.

The strategy for follow up on the preliminary measurements is to obtain new double-polished CGA samples and to deposit Mg or Ca contacts in small patterns on both sides of the sample. Measurements will be conducted both across the sample surface from contact to contact and through the thickness of the CGA. If a reproducible contact pair showing good photoconductivity through the thickness of the sample can be obtained, these will be tested for x-ray and gamma ray sensitivity.

Measurements will be conducted as a function of temperature to determine how the behavior of the contacts changes as the temperature is reduced. This will also supply information about the Schottky barrier height.

## 6.0 Strategy and Future Direction

Based on the progress made in FY07 the strategy and future direction of the project are discussed.

### 6.1 Strategy

Materials processing techniques for synthesizing bulk amorphous semiconductors from Cd-Ge-As glass were developed in FY06, and refined in FY07. Initial DC ionization experiments (with Cd-Ge-As and As-Se/As-Se-Te systems) using sealed alpha sources demonstrated radiation response with three different glass systems in FY07. The next major objective of FY08 is to characterize the transient response of these materials to radiation at RT to determine their performance envelope as gamma radiation detectors. Suitable electronic monitoring tools have been identified and purchases are in progress to acquire them.

### 6.2 Future Direction

Diode-based radiation detectors will be built and tested from amorphous Cd-Ge-As and As-Se-Te materials. These devices will be tested in DC ionization and in pulse mode to determine their performance characteristics. The development of Schottky contacts for Cd-Ge-As glasses is expected to enable room temperature operation of these materials, and take advantage of their higher mobility. We anticipate that detector performance will be impeded by slow charge carrier transport issues. We have developed a three-pronged approach to address this issue.

- First, processing, composition, and H-doping will be used to reduce the density of defect states.
- Second, high fields will be used to fill trap states and also accelerate charge carriers sufficiently to promote cascading and avalanche effects to compensate for lost/trapped charge carriers.
- Finally, photolithographic patterning will be used to create arrays of pixilated FET structures with Schottky barrier contacts and short charge carrier transit paths to minimize collection times.

Based on these results, we foresee three future potential applications of these materials. One application would be the creation of a 2-D array of small FET structures with pairs of biased Schottky diode contacts that create a high field in the small area between the contacts. This would result in a position sensitive radiation detector with quasi imaging capabilities. The second application would be to exploit the charge carrier amplification and low leakage current properties of these materials and build low-noise avalanche photo-diodes out of them. The third potential application would be to use them in bulk form, as a traditional semiconductor detector. Charge carrier mobility and trapping issues may limit overall detector volume, however more experiments and characterization studies are needed to better bound the operating envelope.

## 7.0 References

- (1) Rud, V.; Rud, Y.; Poluushina, I.; Ushakova, T.; Iida, S., "Observation of Record Electron Hall Mobility in CdGeAs<sub>2</sub> Single Crystals," *Jpn. J. Appl. Phys.*, 39 [Suppl. 39-1] 266-267 (2000).
- (2) Rud, V. Y.; Rud, Y. V.; Pandey, R.; Ohmer, M. C., "Evidence of high electron mobility in CdGeAs<sub>2</sub> single crystals"; pp. 439 in *Infrared Applications of Semiconductors III. Symposium (Materials Research Society Symposium Proceedings Vol.607)*, Edited by Mater. Res. Soc, Boston, MA, USA, 2000.
- (3) Roy, U. N.; Groza, M.; Cui, Y.; Burger, A.; Bell, Z. W.; Carpenterl, D. A., "Crystal growth, characterization and fabrication of AgGaSe<sub>2</sub> crystals as a novel, material for room-temperature radiation detectors"; pp. 177 in *Proceedings of SPIE - The International Society for Optical Engineering*, Vol. 5540. Edited by International Society for Optical Engineering, Bellingham, WA 98227-0010, United States, Denver, CO, United States, 2004.
- (4) Hruby, A.; Stourac, L., "Semiconducting glasses based on CdAs<sub>2</sub>," *Materials Research Bulletin*, 4 [10] 745-756 (1969).
- (5) Risbud, S. H., "Processing and properties of some II-IV-V<sub>2</sub> amorphous and crystalline semiconductors," *Applied Physics A: Materials Science & Processing*, 62 [6] 519 (1996).
- (6) Stourac, L., "Thermal conductivity of semiconducting amorphous CdGeAs<sub>2</sub>," *Czech. J. Phys.*, V19 [5] 681-684 (1969).
- (7) Kokorina, V. F., *Glasses for infrared optics*. CRC Press, Boca Raton, FL, 1996.
- (8) Vengel, T. N.; Kolomiets, B. T., "Vitreous Semiconductors, some properties of materials in the As<sub>2</sub>Se<sub>3</sub> - As<sub>2</sub>Te<sub>3</sub> System II," *Soviet Physics Technical Physics*, 2 2314-2319 (1957).
- (9) Mahadevan, S.; Giridhar, A.; Rao, K. J., "Study of electron transport in As-Se-Te glasses," *J. Phys. C: Solid State Phys.*, 10 4499-4510 (1977).
- (10) Hong, K. S.; Berta, Y.; Speyer, R. F., "Glass-crystal transition in II-IV-V<sub>2</sub> semiconducting compounds," *Journal of the American Ceramic Society*, 73 [5] 1351 (1990).